




Photon and phonon statistics in a qubit-plasmon-phonon ultrastrong-coupling systemTing-ting Ma ¹, Dmitri B. Horoshko ², Chang-shui Yu ^{1,3,*} and Sergei Ya. Kilin²¹*School of Physics, Dalian University of Technology, Dalian 116024, China*²*B. I. Stepanov Institute of Physics, NASB, Nezavisimosti Avenue 68, Minsk 220072, Belarus*³*DUT-BSU Joint Institute, Dalian University of Technology, Dalian 116024, China*

(Received 23 December 2021; accepted 2 May 2022; published 31 May 2022)

We study the photon and phonon statistics of a qubit-plasmon-phonon hybrid system in the ultrastrong-coupling regime. The introduced qubit coupling causes parity-conserving and -nonconserving situations. We employ an analytic approximation approach for the parity-conserving case to reveal the statistical behaviors of photons and phonons. It indicates that both photons and phonons show strong antibunching at the same frequency. Even though the bunching properties of photons and phonons occupy the dominant regions of the considered frequencies, phonons tend to weak antibunching within the photonic strong-bunching area. In contrast, one can find that the configurations of correlation functions for both photons and phonons in the parity-conserving case are squeezed towards the central frequency by parity breaking, which directly triggers the reverse statistical behaviors of the different parties in the low-frequency regions and the strong-bunching properties in other frequency regions. The photon-phonon cross-correlation function also demonstrates similar parity-induced differences, indicating that the nonconserving parity induces the photon-phonon bunching behavior. We finally analyze the delayed second-order correlation function with different driving frequencies, which illustrates striking oscillations revealing the occurrence of simultaneous multiple excitations.

DOI: [10.1103/PhysRevA.105.053718](https://doi.org/10.1103/PhysRevA.105.053718)**I. INTRODUCTION**

Photon blockade has received much attention in recent years due to the nonclassical behavior of the quantum emitter, which leads to the realization of single-photon sources and single-photon detectors [1–7]. Photon blockade is the nonlinear excitation of the first photon with a high probability of blocking the transmission of the second photon [8,9] so that the emitted photons have a strong antibunching trend. With nanotechnologies, phonon lasers and single-photon generations have attracted wide interest. In particular, photons and phonons exhibit mutual antibunching in their correlated behavior in some photon-phonon hybrid systems. The output photon, phonon, or their correlated statistics can be characterized by the equal-time second-order correlation function $g^{(2)}(0)$ and two-time correlation function $g^{(2)}(\tau)$, which can reveal nonclassical characters of the fields [10,11].

Cavity quantum electrodynamics is a powerful platform for studying the interactions between light and matter and between photons. The typical candidate is the Jaynes-Cummings model. In such a qubit-cavity system, the ratio of the qubit-cavity coupling constant g and the cavity-mode frequency ω_0 characterizes the coupling strength η , which is closely related to the nonlinear effects in the system [12,13]. In recent years, the ultrastrong-coupling regime with $\eta > 0.1$ was achieved [12–21]. In this regime, the rotating-wave approximation is no longer valid, which has many intriguing physical effects [22–27], and extensive research has been carried out

regarding the modification of weak-coupling quantum phenomena [28–32]. In particular, it was found that parametric processes induced by strong coupling can greatly influence photon blockade [3]. Recently, it was also shown that one photon could simultaneously excite two or more atoms in the ultrastrong-coupling regime [34]. These effects in the ultrastrong-coupling regime can open up applications in quantum information processing [27,31,33].

Ultrastrong plasmon-phonon coupling has been realized via epsilon-near-zero (ENZ) nanocavities, which can drastically reduce the size of the system and thus the amount of material involved in the realization of midinfrared ultrastrong coupling [35]. It has been shown that the coupling strength between the ENZ mode of the cavity and the SiO₂ phonon with a normalized coupling strength can be larger than 0.25. In particular, it provides a different form of photon and phonon coupling in experiments, where the coaxial ENZ mode is coupled to the lattice vibrations of SiO₂ in a manner different from the traditional optomechanical coupling mechanism. In addition, the ENZ nanocavity has also been designed and studied in many aspects [36–43], which can provide a different way to explore the quantum nonlinear optical processes.

This paper theoretically studies photon (phonon) statistics in the ENZ nanocavity, especially concerning the optomechanical coupling mechanism. To investigate the nonlinear optical effects, we introduce a single two-level atom into the ultrastrong photon-phonon coupling regime and show the photon and phonon statistics in the parity-conserving and -nonconserving cases induced by the atom-photon coupling. The nonlinearity of the cavity is mediated by the two-level atom. In such an ultrastrong-coupling regime,

*yys@dut.edu.cn

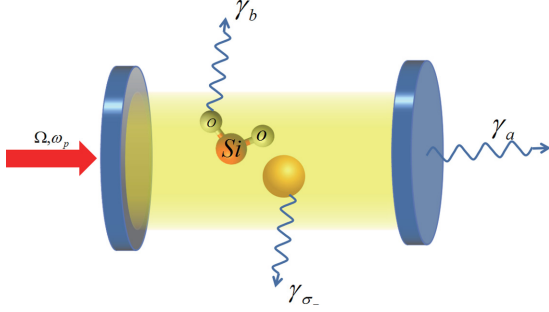


FIG. 1. Schematic diagram of the coherently driving qubit-plasmon-phonon hybrid nanocavity. The driving strength is Ω ; the driving frequency is ω_d . The coupling of the plasmon mode and SiO₂ phonon mode is ultrastrong. γ_{σ^-} and γ_b are the spontaneous emission rates of the qubit and phonon, respectively, and γ_a is the decay rate of the cavity.

all counterrotating-wave contributions should not be neglected [12,13], and the equal-time correlation function $g^{(2)}(0)$ and two-time correlation function $g^{(2)}(\tau)$ will also be changed in comparison with the usual forms [3,5]. We find that in the parity-conserving case, photons and phonons demonstrate strong antibunching behavior at the same driving frequency ω_d and approach a coherent state in the high-frequency region $\omega_d \in [1.3\omega_0, 1.4\omega_0]$. In the middle-frequency region $\omega_d \in [0.9\omega_0, 1.15\omega_0]$, photons tend to strong bunching, but phonons are inclined to weakly antibunch. Interestingly, nonconserving parity leads to the shift in eigenenergies. As a result, the configurations of correlation functions $g^{(2)}(0)$ and intensities (average particle numbers) are squeezed towards the middle-frequency region, which leads to quite different and even opposite statistical behaviors compared with the parity-conserving case. Within the range of relatively high frequencies $\omega_d \in [1.2\omega_0, 1.4\omega_0]$, the photons and phonons are more inclined to bunch in the parity-nonconserving case. In addition, the delayed second-order correlation functions from different driving frequencies illustrate striking oscillations, which reveals simultaneous multiple excitations. The remainder of this paper is organized as follows. Section II introduces our considered model and derives the corresponding dynamical equation. In Sec. III, we employ an analytic approximation to study the photon and phonon statistics in the parity-conserving case. In Sec. IV, we mainly consider the parity-nonconserving case. We finally give the conclusions and a discussion in Sec. V. The introduced qubit coupling can lead to parity-conserving and parity-nonconserving situations. In each case, we study the photon statistics of the plasmon mode, the phonon statistics of the SiO₂ vibrations, and their cross correlation characterized by the cross-correlation function $g_{ab}^{(2)}(0)$.

II. MODEL AND DYNAMICS

We consider a hybrid system consisting of an embedded qubit and an ENZ nanocavity with ultrastrong plasmon-phonon coupling. The schematic diagram is sketched in Fig. 1, where the ENZ nanocavity is fabricated by the vibrational ultrastrong coupling of the plasmon mode and the SiO₂ phonon [35,44]. Especially, we suppose that the plasmon

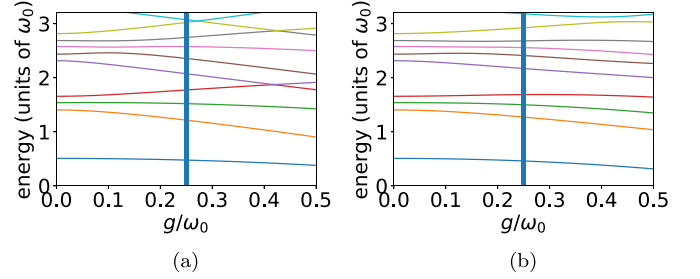


FIG. 2. Energy spectra of the qubit-plasmon-phonon hybrid system as a function of the coupling strength g (a) for $\theta = \pi/2$ and (b) for $\theta = \pi/4$. The vertical line marks coupling strength $g = 0.25\omega_0$.

modes are linearly coupled to a qubit [3,34–36]. The Hamiltonian of the whole ultrastrong-coupling qubit-plasmon-phonon hybrid system reads $H_s = H_0 + H_{\text{int}}$, where

$$H_0 = \omega_0(a^\dagger a + \frac{1}{2}) + \omega_{\text{TO}}(b^\dagger b + \frac{1}{2}) + \frac{1}{2}\omega\sigma_z \quad (1)$$

corresponds to the free Hamiltonian ($\hbar = k_B = 1$) of the photon, phonon, and qubit with ω_0 , ω_{TO} , and ω representing their corresponding frequencies, respectively,

$$H_{\text{int}} = ig_C(a + a^\dagger)(b - b^\dagger) + g_D(a + a^\dagger)^2 + g(a + a^\dagger)[\cos(\theta)\sigma_z - \sin(\theta)\sigma_x] \quad (2)$$

represents the photon-phonon interaction and the interaction between the photon and the qubit [35,45–47], with

$$g_C = \frac{\omega_p}{2} \sqrt{\frac{\omega_{\text{TO}}}{\omega_0}}, \quad g_D = \frac{\omega_p^2}{4\omega_0} \quad (3)$$

denoting the coupling constants of the plasmon-phonon interaction and a (a^\dagger) and b (b^\dagger) being the annihilation (creation) operators of the photons and phonons. Nevertheless, the term related to g_D contains only photon operators due to the squared electromagnetic vector-potential part of the light-matter interaction [46]. Meanwhile, g describes the strength of the coupling between the qubit and photon or phonon mode [48]. θ is a crucial physical quantity that has a significant impact on the spectra and the transitions of the qubit-plasmon-phonon system [14]. Note that there is no direct coupling between the qubit and phonons, which is quite different from the fully coupled hybrid cavity optomechanics [49]. The system is parity conserved for $\theta = \pi/2$, which can be seen from the fact that the parity of the system $\Pi = -\sigma_z \exp(i\pi\hat{N})$, with $\hat{N} = a^\dagger a + b^\dagger b$, commutes with the Hamiltonian H_s , i.e., $[H_s, \Pi] = 0$ [22]. The parity is determined by the total excitation number. The even excitations have odd parity corresponding to the -1 eigenvalue of Π , and the odd excitations have even parity corresponding to $+1$. Obviously, the ground state has even parity. Transitions between the states in the same parity space are forbidden because the transitions induced by the operators $a - a^\dagger$, $b - b^\dagger$, and $\sigma - \sigma^\dagger$ will alter the parity of the state [30]. The energy levels versus the coupling strength are plotted in Fig. 2 for both the parity-conserving ($\theta = \pi/2$) and parity-nonconserving ($\theta = \pi/4$) cases. We are mainly interested in coupling strength $g = 0.25\omega_0$, which is explicitly marked in Fig. 2. It can be seen from Fig. 2 that the cross points among the

spectra occur with the increase of the coupling strength in the parity-conserving case. Therefore, the coupling strength g is crucial to the spectra in this hybrid system. It can affect the transition of the system and the parity of each state [3,30]. Compared with the parity-nonconserving case, the energy levels of the same photon (phonon) state are sparser when $\theta = \pi/2$. Considering coherent driving on the plasmon cavity mode as

$$H_d = \Omega \cos(\omega_d t)(a + a^\dagger) \quad (4)$$

with driving frequency ω_d and driving strength Ω , the total Hamiltonian of this driven hybrid system is given by $H_{\text{total}} = H_s + H_d$.

Since the hybrid system is within the ultrastrong-coupling and weak-driving regime, local treatments on each subsystem like individual dissipations cannot be a good approximation anymore. They could lead to wrong results [50–54], which means that the local Lindblad master equation cannot describe the dynamics of the system well. So we have to employ the global (nonlocal) master equation to study the dynamics [50,55]. Now we follow the standard process to derive the global master equation [55] and first turn to the H_s representation. Based on the eigendecomposition $H_s = E_i|i\rangle\langle i|$, with E_i and $|i\rangle$ corresponding to the eigenenergies and eigenstates, respectively, one can find H_d in the H_s representation as

$$H_d = \Omega \cos(\omega_d t) \left[\sum_{j,k>j} \langle j|(a^\dagger + a)|k\rangle|j\rangle\langle k| + \text{H.c.} \right]. \quad (5)$$

Thus, the global master equation can be derived as [28,55]

$$\dot{\rho}(t) = i[\rho(t), H_{\text{tot}}] + \sum_{j,k>j} \sum_{c=a,b,\sigma_-} \Gamma_c^{jk} D_{|j\rangle\langle k|}[\rho], \quad (6)$$

where

$$D_{|j\rangle\langle k|}[\rho] = |j\rangle\langle k|\rho|k\rangle\langle j| - \frac{1}{2}(|k\rangle\langle k|\rho + \rho|k\rangle\langle k|) \quad (7)$$

is the dissipator and $\Gamma_c^{jk} = \gamma_c \frac{\Delta_{kj}}{\omega_0} |C_{jk}^c|^2$, with $C_{jk}^c = -i\langle j|(c - c^\dagger)|k\rangle(c = a, b, \sigma_-)$ and $\Delta_{kj} = E_k - E_j$, denote the relaxation coefficients corresponding to the transition induced by c [3]. In addition, the parameters used in this paper show that all transition frequencies are different. Here we would like to emphasize that all the transition operators are given by the dressed-state basis, which indicates the collective roles of the cavity, the atom, and the phonon. This should be distinguished from the local master equation, which is usually valid only for $\omega_0, \omega_{\text{TO}}, \omega \gg g_c, g_D, g \sim \gamma_c$, i.e., the weak internal coupling.

III. PARITY-CONSERVING CASE

In order to reveal the photon and phonon statistics, we will consider the equal-time correlation function $g^{(2)}(0)$. In the traditional treatment of the field emitted by a cavity with the photon annihilation operator a and decay rate γ , its positive-frequency part is represented by the operator $a_{\text{out}} = a_{\text{in}} + \sqrt{\gamma}a$, where a_{in} is the vacuum field impinging on the cavity mirror from the outside [56]. This means that a click of an external detector corresponds to annihilation of an intracavity photon. In the case of several interfering bosonic modes, the operator a should be replaced by a weighted sum of the

boson annihilation operators of these modes [57]. In the case of ultrastrong coupling, however, the operator a in the above expression should be replaced by the positive-frequency part of the intracavity field \dot{X}^+ , which has a more complicated form [3]. We make such replacements for the photon and phonon fields and consider the modified $g_c^{(2)}(\tau)$ as [3,58,59]

$$g_c^{(2)}(\tau) = \lim_{t \rightarrow \infty} \frac{\langle \dot{X}_c^-(t)\dot{X}_c^-(t+\tau)\dot{X}_c^+(t+\tau)\dot{X}_c^+(t) \rangle}{\langle \dot{X}_c^-(t)\dot{X}_c^+(t) \rangle^2}, \quad (8)$$

where $\dot{X}_c^+ = \sum_{j,k>j} Y_{jk}|j\rangle\langle k|$ is the c -related operator given in the H_s representation with

$$Y_{jk} = -i\Delta_{kj}\langle j|(c - c^\dagger)|k\rangle, \quad c = a, b. \quad (9)$$

It is obvious that $\tau = 0$ in Eq. (8) defines the equal-time correlation function $g_c^{(2)}(0)$. In addition, one can get $\dot{X}_c^+|0\rangle = 0$, which corresponds to the annihilation operator in the weak- and strong-coupling regimes [16]. The intensity of the output photon or phonon flux emitted by a resonator can be represented by $n_c = \langle \dot{X}_c^- \dot{X}_c^+ \rangle$ [34,60].

To proceed, let us first focus on the special case with $\theta = \pi/2$, in which the parity of the system is conserved [3]. Since we are interested in only the weak driving limit $\Omega \ll \omega_0, g$, the multiple-photon (phonon) processes correspond to the high order of Ω , which allows us to consider our model by truncating different photon (phonon) numbers. For example, let us consider a simple case of N photons and N phonons. According to the spectra and the allowable transitions of the hybrid system in Fig. 2, one can find that the transitions between the ground state $|0\rangle$ and the excited states $|j\rangle$ with $j = 1, 2, 3$ correspond to the single-photon process, and the transitions between the ground state $|0\rangle$ and the excited states with $j = 4, 5, 6, 7, 8$ correspond to the double-photon process and so on. Let the bare states $|n_a, n_b, e(g)\rangle$ correspond to photonic and phononic modes and the qubit; then state $|j\rangle$ can be spanned as $|j\rangle = \sum_{n_a, n_b, n_c} \tilde{C}_{n_a n_b n_c} |n_a, n_b, n_c\rangle$, with $n_c = 1$ or 0 denoting the qubit's excited or ground state $|e(g)\rangle$. One can find that state $|j\rangle$ with $j \in \{k^2, \dots, k^2 + 2k\}$ for $k \leq N$ and $j \in \{f(k), \dots, f(k-1) - 1\}$ with $f(k) = N^2 - (N-k)(3N-k+1)$ for $N \leq k \leq 2N-1$ denotes k excitations from the ground state $|0\rangle$. We would like to emphasize that the ground state $|0\rangle$ is not a vacuum state but a dressed state superposed by the bare states. Essentially, this is attributed to the counterrotating-wave terms, as well as the squared vector potential, which break the conservation of the excitation number in this ultrastrong-coupling regime [12,27].

Due to the weak driving with $\Omega \ll \omega_0, \omega, g, \Delta_{nm}$, we assume that the driving field does not change the eigenstate of the hybrid system, so the rotating-wave approximation can be safely taken over H_d . Thus, the total Hamiltonian in the H_s representation reads

$$H_{\text{total}}(t) = \sum_{n=0} E_n \sigma_{nn} + \left(\sum_{n>m} K_{mn} \sigma_{mn} e^{i\omega_d t} + \text{H.c.} \right), \quad (10)$$

where the second term corresponds to H_d , $K_{mn} = \frac{\Omega}{2} \langle m|a + a^\dagger|n\rangle$, and $\sigma_{mn} = |m\rangle\langle n|$.

If we perform a unitary transformation on the Hamiltonian $H_T = U^\dagger H_s(t) U$, with

$$U = \exp \left[-it \sum_{m=0} (\mathcal{K} \omega_d) \sigma_{mm} \right], \quad (11)$$

with $\mathcal{K} = 0, 1, 2, \dots$ corresponding to $m \in \{\mathcal{K}^2, \dots, (\mathcal{K} + 1)^2 - 1\}$, the time dependence of the total Hamiltonian of the system will be eliminated [5] as

$$H_T = \sum_{n=1} (\Delta_{n0} - \mathcal{K} \omega_d) \sigma_{nn} + \sum_{n>m} (K_{mn} \sigma_{mn} + \text{H.c.}). \quad (12)$$

Now we can employ an approach similar to that in Ref. [61] to deal with the dynamics with dissipations. When no quantum jumps occur, the evolution of the system is governed by the non-Hermitian effective Hamiltonian [62]

$$H_{\text{eff}} = H_T - \frac{i}{2} \sum_{j=1} \Gamma_j |j\rangle \langle j|. \quad (13)$$

In this sense, the dynamics of the qubit-plasmon-phonon hybrid system can be described by the Schrödinger equation $i \frac{\partial \Psi(t)}{\partial t} = H_{\text{eff}} |\Psi(t)\rangle$. With the N^2 -state truncation, $|\Psi(t)\rangle$ can be expanded as

$$|\Psi(t)\rangle = \sum_{j=0}^{N^2-1} C_n(t) |j\rangle, \quad (14)$$

which leads to the following equations for the probability amplitudes:

$$\dot{C}_j = \lambda_{j\mathcal{K}} C_j + \sum_{\text{odd } k \leq N} \sum_{n=k^2}^{k^2+2k} K_{0n} C_n, \quad j \in [\mathcal{K}^2, \mathcal{K}^2 + 2\mathcal{K}], \quad (15)$$

where k takes odd or even numbers for even or odd $\mathcal{K} \in [0, N - 1]$, respectively; $\lambda_{j\mathcal{K}} = \Delta_{j0} - \mathcal{K} \omega_d - \frac{i\Gamma_j}{2}$, with $\Gamma_j = \sum_{k=(\mathcal{K}-1)^2}^{\mathcal{K}^2} \sum_{c=a,b,\sigma_-} \Gamma_c^{jk}$ for $j \in [\mathcal{K}^2, \mathcal{K}^2 + 2\mathcal{K}]$.

Since the driving field is weak enough, the hybrid system will stay in the ground state with a probability of almost 1, which can be explicitly illustrated by the populations of the lower nine eigenstates plotted in Fig. 3, where all the parameters are selected within the current experimental conditions [35,63]. Note that the population $|C_j|^2$ at $\omega_d \approx 1.05\omega_0$ is about two orders of the magnitude lower than the population $|C_1|^2$ at $\omega_d \approx 0.74\omega_0$ in Fig. 3(b). This is also the reason why the population $|C_0|^2$ in Fig. 3(a) has no apparent decrease at $\omega_d \approx 1.05\omega_0$. In order to give an explicit solution, we take $N = 3$ for an example. Thus, the above equations for steady states can be completely solved, and we can obtain

$$C_1 = \frac{\mathcal{M}_{23} - \mathcal{M}_{12}}{\mathcal{N}_{12} - \mathcal{N}_{23}}, \quad (16)$$

$$C_2 = \mathcal{M}_{12} + \mathcal{N}_{12} C_1, \quad (17)$$

$$C_3 = -\frac{K_{01} C_1 + K_{02} C_2}{K_{03}}, \quad (18)$$

$$C_j = -\frac{\sum_{k=1}^{k=3} K_{jk} C_k}{\lambda_{j2}}, \quad 4 \leq j \leq 8, \quad (19)$$

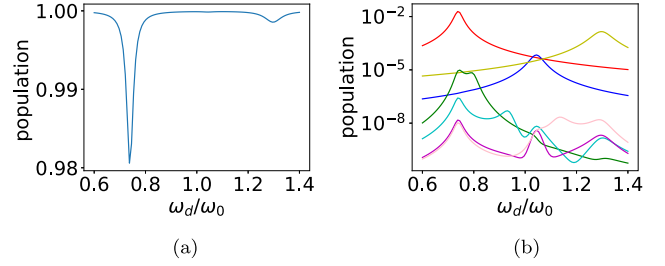


FIG. 3. Populations of (a) the ground state and (b) the lower eight excited states. Here $\theta = \pi/2$, $g = 0.25\omega_0$, $\Omega = 5 \times 10^{-3}\omega_0$, $\gamma_a = \gamma_b = \gamma_{\sigma_-} = 5 \times 10^{-2}\omega_0$, $\omega_p = 0.25\omega_0$, $\omega = \omega_0 + 2g_D$, $\omega_{T0} = \omega$. (a) shows that the excitation becomes strong at $\omega_d = \Delta_{10} \approx 0.74\omega_0$, $\omega_d = \Delta_{20} \approx 1.04\omega_0$, and $\omega_d = \Delta_{30} \approx 1.3\omega_0$. (b) Curves from top to bottom at $\omega_d = 0.6\omega_0$ correspond to state $|j\rangle$, $j = 1, 2, \dots, 8$. Note that all the parameters in the following figures, if not specified, are the same as defined here.

where

$$\mathcal{M}_{mn} = \frac{A_{m3} K_{n0} - A_{n3} K_{m0}}{A_{m2} A_{n3} - A_{m3} A_{n2}}, \quad (20)$$

$$\mathcal{N}_{mn} = \frac{A_{m3} A_{n1} - A_{m1} A_{n3}}{A_{m2} A_{n3} - A_{m3} A_{n2}}, \quad (21)$$

with

$$A_{mn} = -\sum_{j=4}^{j=8} \frac{K_{mj} K_{jn}}{\lambda_{j2}}. \quad (22)$$

Substituting C_n into Eq. (14), we can obtain the state $|\Psi(+\infty)\rangle$. Thus, the equal-time second-order correlation function of Eq. (8) can be directly calculated for photons as

$$g_a^{(2)}(0) = \frac{|\sum_{n=4}^8 \sum_{j=1}^3 Y_{nj} Y_{j0} C_n|^2}{\langle n_a \rangle^2}, \quad (23)$$

with the mean photon number $\langle n_a \rangle$ given by

$$\langle n_a \rangle = \left| \sum_{n=1}^3 Y_{n0} C_n \right|^2 + \sum_{j=1}^3 \left| \sum_{n=4}^8 Y_{nj} C_n \right|^2. \quad (24)$$

Note that $g_b^{(2)}(0)$ can also be obtained similarly, and for a precise solution, we can solve the equations with large N . But the solution is tedious, so we do not explicitly provide it here.

To provide an illustration of the statistical behaviors, we plot the equal-time second-order correlation functions $g_a^{(2)}(0)$ and $g_b^{(2)}(0)$ for photons and phonons, respectively, in Fig. 4. As a comparison, we plot the results from numerically solving the master equation (6) [64] and the analytic results from solving equations similar to Eq. (15). Here we consider the state space with five photons and five phonons as an example. It is shown that our analytic method and the numerical simulation are in good agreement. We can find that there is a deep trough at $\omega_d \approx 0.74\omega_0$ in Figs. 4(a) and 4(c), respectively, which indicates the evident photon and phonon antibunching. This corresponds to the resonantly driving transition from $|0\rangle$ to $|1\rangle$ via a single-excitation process, which blocks the second excitation with a high probability and hence demonstrates antibunching in both figures so that the photons and phonons

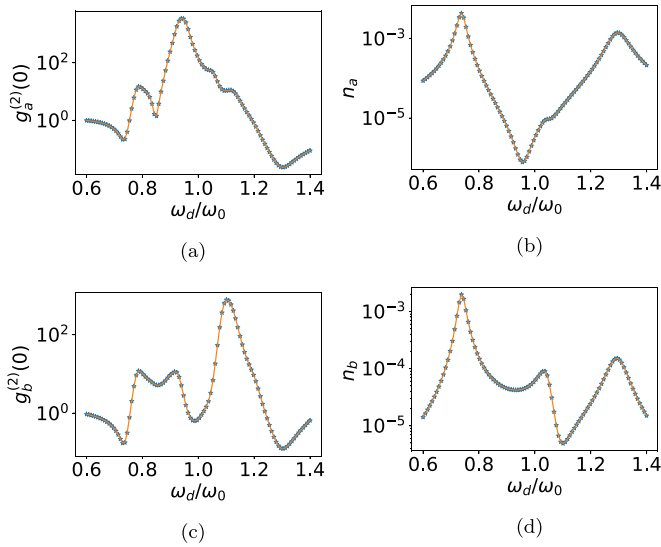


FIG. 4. Equal-time second-order correlation functions of (a) photons $g_a^{(2)}(0)$ and (c) phonons $g_b^{(2)}(0)$ and the number of (b) photons n_a and (d) phonons n_b . The red solid line represents the analytic results given in Eq. (23), and the stars are given by the numerical solution of Eq. (6).

tend to appear in the nanocavity one by one. At $\omega_d \approx 1.3\omega_0$, both photons and phonons approach the Poisson distribution. Meanwhile, these phenomena are accompanied by the relatively large intensity of the output photon and phonon flux, as shown in Figs. 4(b) and 4(d). In Fig. 4(a) there are four apparent peaks at $\omega_d \approx 0.8\omega_0, 0.94\omega_0, 1.05\omega_0, 1.13\omega_0$ corresponding to the double-photon resonant driving transitions from $|0\rangle$ to $|4\rangle$, respectively, which shows the photon bunching tendency. Similarly, at the four frequencies, we can see from Fig. 4(c) that phonons have similar bunching behaviors. The reason is that the bare basis spanning the five eigenstates $|4\rangle, \dots, |5\rangle$ are symmetric on photons and phonons and especially lead to comparable transition rates for photons and phonons. One significant difference is that phonons demonstrate the weak-antibunching behavior around $\omega_d \approx 1.0\omega_0$, accompanied by a slightly enhanced phonon flux. It can be understood that the driving field resonant with the frequency ω_0 of the cavity mode excites the photons in the cavity with a large probability; meanwhile, the strong optomechanical coupling induces a high probability of one-to-one photon-phonon conversion, which mainly corresponds to a single-phonon excitation. In this sense, the statistical properties of photons and phonons in the considered frequency region are roughly similar in the parity-conserving case, but their details are different and even opposite around $\omega_d \approx 1.0\omega_0$.

IV. PARITY-NONCONSERVING CASE

In the previous section, we employed an analytic approximation method to investigate the photon and phonon statistics in the parity-conserving case. However, in the parity-nonconserving case, the transitions will become a little complicated [14] and cannot be easily dealt with by a universal analytic treatment. So we will use a numerical process to study the correlation functions. In the following, we

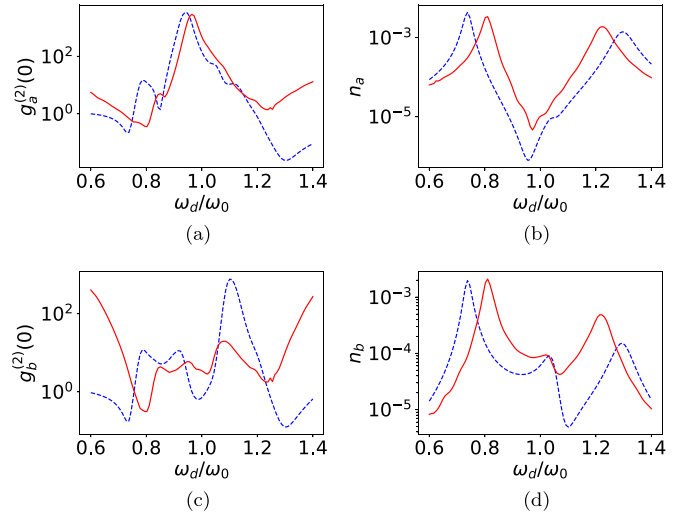


FIG. 5. Equal-time second-order correlation functions of (a) photons $g_a^{(2)}(0)$ and (c) phonons $g_b^{(2)}(0)$ and the number of (b) photons n_a and (d) phonons n_b . The blue dashed line and the red solid line correspond to $\theta = \pi/2$ and $\theta = \pi/4$, respectively.

will find more striking physical effects with changing θ . In Fig. 5, we plot the second-order correlation functions for both $\theta = \pi/4$ and $\theta = \pi/2$ and the intensities of the output flux ($n_c, c = a, b$) for $\theta = \pi/4$ versus the driving frequency ω_d . Compared with the conserved parity, the obvious phenomenon in Fig. 5 is that the configurations of both the correlation functions and the intensities are squeezed from two sides to the central frequency $\omega_d \approx \omega_0$, which further leads to quite different and even opposite statistical behaviors. For example, the most typical is that around $\omega_d \approx 0.74\omega_0$ ($0.8\omega_0$), the strong antibunching (bunching) of both photons and phonons switches to the opposite statistical behavior. The intensities of output flux are modestly increased in the middle range of frequencies and slightly decreased in the other range. This reason is that the nonconserving parity induces the eigenenergy translation to change the transition frequencies. For example, the transition $|0\rangle \rightarrow |1\rangle$ is resonant with $\omega_d \approx 0.74\omega_0$ in the parity-conserving case but resonant with $\omega_d \approx 0.8\omega_0$ if the parity is broken. In addition, within the range of relatively high frequencies, the bunching behaviors are greatly enhanced, which shows that the photons and phonons are more inclined to be bunching in the parity-nonconserving case, which is caused by the change in the transitions. For example, when we set an excited state in $|3\rangle$ by resonantly driving $|0\rangle \rightarrow |3\rangle$, the system is able to transit through $|3\rangle \rightarrow |2\rangle \rightarrow |1\rangle \rightarrow |0\rangle$ instead of only $|3\rangle \rightarrow |0\rangle$ as $\theta = \pi/2$, which tends to cause photon bunching.

In order to further study the statistical behaviors of photons and phonons, in Fig. 6 we plot the cross-correlation function $g_{ab}^{(2)}(0)$ [3,65], which is defined as

$$g_{ab}^{(2)}(0) = \frac{\langle \dot{X}_a^- \dot{X}_b^- \dot{X}_b^+ \dot{X}_a^+ \rangle}{\langle \dot{X}_a^- \dot{X}_a^+ \rangle \langle \dot{X}_b^- \dot{X}_b^+ \rangle}. \quad (25)$$

Similar to the usual $g^{(2)}(0)$, $g_{ab}^{(2)}(0) < 1$ indicates that one photon and one phonon do not tend to exist simultaneously; on the contrary, $g_{ab}^{(2)}(0) > 1$ means that the photon and phonon

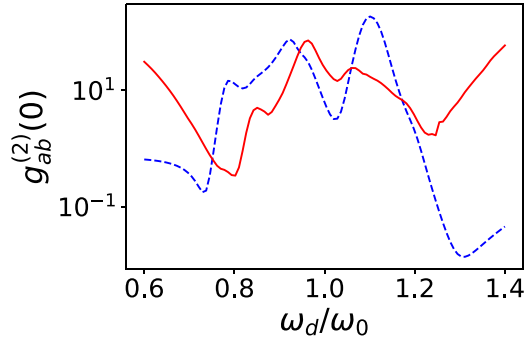


FIG. 6. Cross-correlation function $g_{ab}^{(2)}(0)$. The blue dashed line and the red solid line correspond to $\theta = \pi/2$ and $\theta = \pi/4$, respectively.

tend to bunch together. Roughly speaking, the cross-statistical behaviors of photons and phonons, as shown in Fig. 6, are very similar to the phonons shown in Fig. 5(c). The reason can also be basically understood as being $g_b^{(2)}(0)$, which will not be repeated. But the photon and phonon for the parity-conserving case are inclined to much stronger antibunching at $\omega_d \approx 1.0\omega_0$, which corresponds to driving resonant with the cavity mode. As explained previously, strong optomechanical coupling can induce photon-phonon conversion, but the conserving parity greatly suppresses their simultaneous double excitation, which shows the antibunching behavior of the photon and phonon. However, in the parity-nonconserving case, all the bare bases $|n_a, n_b, e(g)\rangle$ covered in the ground state $|0\rangle$ have a nonzero probability amplitude. Therefore, photons excited by the resonant driving will trigger simultaneous photon and phonon excitation with a relatively large probability. Thus, the photon and phonon tend to stronger bunching at $\omega_d \approx 1.0\omega_0$. In addition, it is worth noting that, when $\omega_d \approx 0.74\omega_0$ ($0.8\omega_0$) in the parity-conserving (parity-nonconserving) case, $g_a^{(2)}(0)$, $g_b^{(2)}(0)$, and $g_{ab}^{(2)}(0)$ are all at the most obvious frequency dips of antibunching, which indicates that at $\omega_d \approx 0.74\omega_0$ photons and phonons in the nanocavity tend to appear one by one with large probability and disentangle from each other [66]. This result has important implications for the detection of phonons and photons [67].

We also study the delayed second-order correlation function $g_a^{(2)}(\tau)$ in three different situations with the driving frequency resonating with the three lower excitations. As can be seen in Fig. 7, when we drive the transitions $|0\rangle \rightarrow |2\rangle$ and $|0\rangle \rightarrow |3\rangle$, they both give rise to noteworthy oscillations of $g_a^{(2)}(\tau)$. Obviously, when we drive $|0\rangle \rightarrow |2\rangle$, $g_a^{(2)}(\tau)$ oscillates between bunching and antibunching at the frequency Δ_{21} . This oscillation originates from the fact that the driving on the transition $|0\rangle \rightarrow |2\rangle$ leads to excitations of both states $|1\rangle$ and $|2\rangle$ separated by Δ_{21} , which is similar to what was given in Ref. [3]. In particular, when driving $|0\rangle \rightarrow |3\rangle$, three excited states can be excited. The $|3\rangle$ and $|1\rangle$ states can be excited with relatively large probability, which leads to the oscillation of $g_a^{(2)}(\tau)$ at the frequency Δ_{31} in a short interval and then further triggers the excitation $|2\rangle$, which leads to the oscillation at the frequency Δ_{21} . The photons are gradually inclined to be photon antibunching in this case. In addition, the oscillations

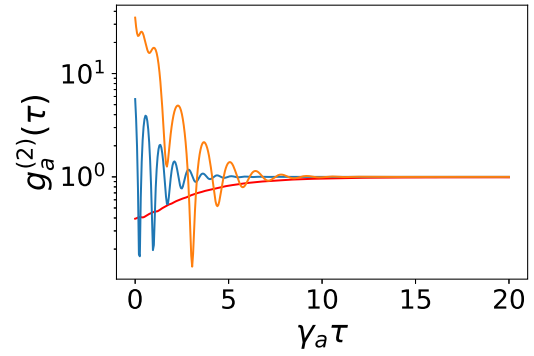


FIG. 7. $g_a^{(2)}(\tau)$ with $\theta = \pi/4$ and ω_d resonant with $|0\rangle \rightarrow |1\rangle$ (red), $|0\rangle \rightarrow |2\rangle$ (blue), and $|0\rangle \rightarrow |3\rangle$ (orange) transitions.

also occur at the beginning in $\omega_d = \Delta_{10}$ with a much lower amplitude.

V. CONCLUSIONS AND DISCUSSION

We have investigated photon and phonon statistics of a coherently driven qubit-plasmon-phonon hybrid system in the ultrastrong-coupling regime. We have considered the parity-conserving and -nonconserving regimes. Except for the regions where photons show strong bunching behaviors and phonons tend to weak antibunching, the statistical behaviors for both phonons and photons are pretty similar in the parity-conserving case. The broken parity essentially leads to the translation of energy levels, which squeezes the correlation function towards the central frequency. This squeezing triggers the opposite statistical behaviors in the low-frequency region and enhances the bunching properties in the medium- and high-frequency regions. A similar phenomenon was also found in the photon-phonon statistics, characterized by their cross-correlation functions. The delayed second-order correlation function with different driving frequencies illustrates the striking oscillations, revealing simultaneous multiple excitations. Finally, we would like to mention that the strong photon-phonon coupling in Eq. (2) was reported for a wafer-scale resonant ENZ nanocavity (see [35] and references therein), and the strong coupling between a qubit and optical fields can also be controlled by the bias flux of the qubit loop (see [3,34] and references therein). Their combination could still be a challenge. However, these strong couplings provide insights into quantum nonlinear optical processes; especially, the nonlinear optical effects of this nanocavity require further research into the exotic implications.

ACKNOWLEDGMENTS

This work was supported by the National Natural Science Foundation of China under Grants No. 12175029, No. 12011530014, and No.11775040 and the Key Research and Development Project of Liaoning Province under Grant No. 2020JH2/10500003. D.B.H. and S.Y.K. were supported by the Belarusian Republican Foundation for Fundamental Research under Grant No. F21TURG-003.

- [1] K. Birnbaum, A. Boca, R. Miller *et al.*, Photon blockade in an optical cavity with one trapped atom, *Nature (London)* **436**, 87 (2005).
- [2] B. Dayan *et al.*, A photon turnstile dynamically regulated by one atom, *Science* **319**, 1062 (2008).
- [3] A. Ridolfo, M. Leib, S. Savasta, and M. J. Hartmann, Photon Blockade in the Ultrastrong Coupling Regime, *Phys. Rev. Lett.* **109**, 193602 (2012).
- [4] Y. Zhang, J. Zhang, and C.-S. Yu, Photon statistics on the extreme entanglement, *Sci. Rep.* **6**, 24098 (2016).
- [5] W.-W. Deng, G.-X. Li, and H. Qin, Photon blockade via quantum interference in a strong coupling qubit-cavity system, *Opt. Express* **25**, 6767 (2017).
- [6] M.-C. Li and A.-X. Chen, A photon blockade in a coupled cavity system mediated by an atom, *Appl. Sci.* **9**, 980 (2019).
- [7] F. Zou, D.-G. Lai, and J.-Q. Liao, Enhancement of photon blockade effect via quantum interference, *Opt. Express* **28**, 16175 (2020).
- [8] J. Fink, M. Goppl, M. Baur *et al.*, Climbing the Jaynes-Cummings ladder and observing its nonlinearity in a cavity QED system, *Nature (London)* **454**, 315 (2008).
- [9] M. A. Sentef, M. Ruggenthaler, and A. Rubio, Cavity quantum-electrodynamical polaritonically enhanced electron-phonon coupling and its influence on superconductivity, *Sci. Adv.* **4**, eaau6969 (2018).
- [10] K. Wang, Q. Wu, Y.-F. Yu, and Z.-M. Zhang, Nonreciprocal photon blockade in a two-mode cavity with a second-order nonlinearity, *Phys. Rev. A* **100**, 053832 (2019).
- [11] C. W. Gardiner and P. Zoller, *Quantum Noise* (Springer, Berlin, 2000).
- [12] A. F. Kockum, A. Miranowicz, S. De Liberato *et al.*, Ultrastrong coupling between light and matter, *Nat. Rev. Phys.* **1**, 19 (2019).
- [13] A. Le Boité, Theoretical methods for ultrastrong light-matter interactions, *Adv. Quantum Technol.* **3**, 1900140 (2020).
- [14] Q. Bin, X.-Y. Lü, T.-S. Yin, Y. Li, and Y. Wu, Collective radiance effects in the ultrastrong-coupling regime, *Phys. Rev. A* **99**, 033809 (2019).
- [15] T. Schwartz, J. A. Hutchison, C. Genet, and T. W. Ebbesen, Reversible Switching of Ultrastrong Light-Molecule Coupling, *Phys. Rev. Lett.* **106**, 196405 (2011).
- [16] F. Beaudoin, J. M. Gambetta, and A. Blais, Dissipation and ultrastrong coupling in circuit QED, *Phys. Rev. A* **84**, 043832 (2011).
- [17] E. Sanchez-Burillo, D. Zueco, J. J. Garcia-Ripoll, and L. Martin-Moreno, Scattering in the Ultrastrong Regime: Nonlinear Optics with One Photon, *Phys. Rev. Lett.* **113**, 263604 (2014).
- [18] I. Lizuain, J. Casanova, J. J. García-Ripoll, J. G. Muga, and E. Solano, Zeno physics in ultrastrong-coupling circuit QED, *Phys. Rev. A* **81**, 062131 (2010).
- [19] V. Macrì, A. Ridolfo, O. D. Stefano, A. F. Kockum, F. Nori, and S. Savasta, Nonperturbative Dynamical Casimir Effect in Optomechanical Systems: Vacuum Casimir-Rabi Splitting, *Phys. Rev. X* **8**, 011031 (2018).
- [20] A. F. Kockum, A. Miranowicz, V. Macrì, S. Savasta, and F. Nori, Deterministic quantum nonlinear optics with single atoms and virtual, *Phys. Rev. A* **95**, 063849 (2017).
- [21] G. Scaliari *et al.*, Ultrastrong coupling of the cyclotron transition of a 2D electron gas to a THz metamaterial, *Science* **335**, 1323 (2012).
- [22] S. He, C. Wang, Q.-H. Chen, X.-Z. Ren, T. Liu, and K.-L. Wang, First-order corrections to the rotating-wave approximation in the Jaynes-Cummings model, *Phys. Rev. A* **86**, 033837 (2012).
- [23] C. Wang, L.-Q. Wang, and J. Ren, Impact of counter-rotating-wave term on quantum heat transfer and phonon statistics in nonequilibrium qubit-phonon hybrid system, *Chin. Phys. B* **30**, 030506 (2021).
- [24] E. K. Irish, Generalized Rotating-Wave Approximation for Arbitrarily Large Coupling, *Phys. Rev. Lett.* **99**, 173601 (2007).
- [25] X. Cao, J.-Q. You, H. Zheng, and F. Nori, A qubit strongly coupled to a resonant cavity: Asymmetry of the spontaneous emission spectrum beyond the rotating wave approximation, *New J. Phys.* **13**, 073002 (2011).
- [26] X. Cao, Q. Ai, C.-P. Sun, and F. Nori, The transition from quantum Zeno to anti-Zeno effects for a qubit in a cavity by varying the cavity frequency, *Phys. Lett. A* **376**, 349 (2012).
- [27] T. Niemczyk *et al.*, Circuit quantum electrodynamics in the ultrastrong-coupling regime, *Nat. Phys.* **6**, 772 (2010).
- [28] R. Stassi, A. Ridolfo, O. Di Stefano, M. J. Hartmann, and S. Savasta, Spontaneous Conversion from Virtual to Real Photons in the Ultrastrong-Coupling Regime, *Phys. Rev. Lett.* **110**, 243601 (2013).
- [29] H. Zheng, S.-Y. Zhu, and M. S. Zubairy, Quantum Zeno and Anti-Zeno Effects: Without the Rotating-Wave Approximation, *Phys. Rev. Lett.* **101**, 200404 (2008).
- [30] A. Le Boité, M.-J. Hwang, H. Nha, and M. B. Plenio, Fate of photon blockade in the deep strong-coupling regime, *Phys. Rev. A* **94**, 033827 (2016).
- [31] S. Seah, S. Nimmrichter, and V. Scarani, Refrigeration beyond weak internal coupling, *Phys. Rev. E* **98**, 012131 (2018).
- [32] S. De Liberato, Light-Matter Decoupling in the Deep Strong Coupling Regime: The Breakdown of the Purcell Effect, *Phys. Rev. Lett.* **112**, 016401 (2014).
- [33] M. Pelton, Modified spontaneous emission in nanophotonic structures, *Nat. Photonics* **9**, 427 (2015).
- [34] L. Garziano, V. Macrì, R. Stassi, O. Di Stefano, F. Nori, and S. Savasta, One Photon Can Simultaneously Excite Two or More Atoms, *Phys. Rev. Lett.* **117**, 043601 (2016).
- [35] D. Yoo, F. de León-Pérez, M. Pelton *et al.*, Ultrastrong plasmon-phonon coupling via epsilon-near-zero nanocavities, *Nat. Photonics* **15**, 125 (2021).
- [36] E. L. Runnerstrom *et al.*, Polaritonic hybrid-epsilon-near-zero modes: Beating the plasmonic confinement vs propagation-length trade-off with doped cadmium oxide bilayers, *Nano Lett.* **19**, 948 (2018).
- [37] Q. Zhang, Q. Gong, and Y. Gu, Enhanced photon-emitter coupling in micro/nano photonic structures, *IEEE J. Sel. Top. Quantum Electron.* **27**, 6700310 (2021).
- [38] K. Manukyan *et al.*, Dependence of the coupling properties between a plasmonic antenna array and a sub-wavelength epsilon-near-zero film on structural and material parameters, *Appl. Phys. Lett.* **118**, 241102 (2021).
- [39] S. G. Rodrigo, Amplification of stimulated light emission in arrays of nanoholes by plasmonic absorption-induced transparency, *Opt. Express* **29**, 30715 (2021).

- [40] D. N. Basov, A. Asenjo-Garcia, P. James Schuck, X.-Y. Zhu, and A. Rubio, Polariton panorama, *Nanophotonics* **10**, 549 (2021).
- [41] A. Yadav, R. Kumari, S. K. Varshney, and B. Lahiri, Tunable phonon-plasmon hybridization in α -MoO₃-graphene based van der Waals heterostructures, *Opt. Express* **29**, 33171 (2021).
- [42] A. Thomas *et al.*, Tilting a ground-state reactivity landscape by vibrational strong coupling, *Science* **363**, 615 (2019).
- [43] X. Jin *et al.*, Reshaping the phonon energy landscape of nanocrystals inside a terahertz plasmonic nanocavity, *Nat. Commun.* **9**, 763 (2018).
- [44] J. George, T. Chervy, A. Shalabney, E. Devaux, H. Hiura, C. Genet, and T. W. Ebbesen, Multiple Rabi Splittings under Ultrastrong Vibrational Coupling, *Phys. Rev. Lett.* **117**, 153601 (2016).
- [45] D. J. Shelton *et al.*, Strong coupling between nanoscale metamaterials and phonons, *Nano Lett.* **11**, 2104 (2011).
- [46] C. Ciuti, G. Bastard, and I. Carusotto, Quantum vacuum properties of the intersubband cavity polariton field, *Phys. Rev. B* **72**, 115303 (2005).
- [47] Y. Todorov, and C. Sirtori, Intersubband polaritons in the electrical dipole gauge, *Phys. Rev. B* **85**, 045304 (2012).
- [48] K.-D. Park *et al.*, Tip-enhanced strong coupling spectroscopy, imaging, and control of a single quantum emitter, *Sci. Adv.* **5**, eaav5931 (2019).
- [49] J. Restrepo, I. Favero, and C. Ciuti, Fully coupled hybrid cavity optomechanics: Quantum interferences and correlations, *Phys. Rev. A* **95**, 023832 (2017).
- [50] I. M. Mirza, Strong coupling optical spectra in dipole-dipole interacting optomechanical Tavis-Cummings models, *Opt. Lett.* **41**, 2422 (2016).
- [51] A. F. Alharbi and Z. Ficek, Deterministic creation of stationary entangled states by dissipation, *Phys. Rev. A* **82**, 054103 (2010).
- [52] D. Hu, S.-Y. Huang, J. Q. Liao, L. Tian, and H.-S. Goan, Quantum coherence in ultrastrong optomechanics, *Phys. Rev. A* **91**, 013812 (2015).
- [53] T. Holz, R. Betzholtz, and M. Bienert, Suppression of Rabi oscillations in hybrid optomechanical systems, *Phys. Rev. A* **92**, 043822 (2015).
- [54] J. H. Eberly and K. Wodkiewicz, The time-dependent physical spectrum of light, *J. Opt. Soc. Am.* **67**, 1252 (1977).
- [55] H.-P. Breuer and F. Petruccione, *The Theory of Open Quantum Systems* (Oxford University Press, New York, 2006).
- [56] C. W. Gardiner and M. J. Collett, Input and output in damped quantum systems: Quantum stochastic differential equations and the master equation, *Phys. Rev. A* **31**, 3761 (1985).
- [57] D. B. Horoshko and S. Ya. Kilin, Multimode unraveling of master equation and decoherence problem, *Opt. Express* **2**, 347 (1998).
- [58] C. Noh and H. Nha, Output field squeezing in a weakly-driven dissipative quantum Rabi model, *Opt. Commun.* **435**, 350 (2019).
- [59] C. Ciuti and I. Carusotto, Input-output theory of cavities in the ultrastrong coupling regime: The case of time-independent cavity parameters, *Phys. Rev. A* **74**, 033811 (2006).
- [60] S. De Liberato, D. Gerace, I. Carusotto, and C. Ciuti, Extracavity quantum vacuum radiation from a single qubit, *Phys. Rev. A* **80**, 053810 (2009).
- [61] H. J. Carmichael, R. J. Brecha, and P. R. Rice, Quantum interference and collapse of the wave function in cavity QED, *Opt. Commun.* **82**, 73 (1991).
- [62] I. M. Mirza and S. J. van Enk, Single-photon time-dependent spectra in quantum optomechanics, *Phys. Rev. A* **90**, 043831 (2014).
- [63] M. Barra-Burillo, U. Muniain, S. Catalano *et al.*, Microcavity phonon polaritons from the weak to the ultrastrong phononphoton coupling regime, *Nat. Commun.* **12**, 6206 (2021).
- [64] J. R. Johansson, P. D. Nation, and F. Nori, QuTiP: An open-source Python framework for the dynamics of open quantum systems, *Comput. Phys. Commun.* **183**, 1760 (2012).
- [65] D. F. Walls and G. J. Milburn, *Quantum Optics*, 2nd ed. (Springer, Berlin, 2015).
- [66] H. Kimble, The quantum internet, *Nature (London)* **453**, 1023 (2008).
- [67] M. D. Eisaman, J. Fan, A. Migdall, and S. V. Polyakov, Invited review article: Single-photon sources and detectors, *Rev. Sci. Instrum.* **82**, 071101 (2011).